Electrical Power and Energy Systems 46 (2013) 234–240

Contents lists available at SciVerse ScienceDirect

Electrical Power and Energy Systems

journal homepage: www.elsevier.com/locate/ijepes

Analysis and control of quasi-Z source inverter with battery for grid-connected PV system ☆

Dongsen Sun [a,*], Baoming Ge [a,b], Daqiang Bi [c], Fang Z. Peng [b]

[a] School of Electrical Engineering, Beijing Jiaotong University, Beijing 100044, China
[b] Department of Electrical and Computer Engineering, Michigan State University, MI 48824, USA
[c] Department of Electrical Engineering, Tsinghua University, Beijing 100084, China

ARTICLE INFO

Article history:
Received 2 November 2010
Received in revised form 10 September 2012
Accepted 9 October 2012

Keywords:
Quasi-Z-source inverter
Photovoltaic power generation system
Energy storage system
Grid-tie control

ABSTRACT

The quasi-Z-source inverter (qZSI) has some unique advantages and is suitable for photovoltaic (PV) system. This paper proposes a new topology—a qZSI with battery for PV power generation system. Battery is paralleled with one of the capacitors in quasi-Z-source (qZS) network, instead of an additional DC/DC converter. This system inherits all the advantages of qZSI. Besides, with a battery, the system can smooth the grid-injected power when PV power fluctuates. The operating principle of the new topology is analyzed and the design scheme of the qZS network is presented. And then, closed-loop control strategy for the proposed system is designed to manage the three power flows of PV panel, grid, and battery in the system. Maximum Power Point Tracking (MPPT) has been implemented in the qZSI with battery-based PV system by using the proposed control scheme. Different operating modes are simulated. A small-scale power prototype with a real PV panel is built to test the proposed system. The simulation results and experimental results verify the proposed circuit, theoretical analysis, and the control scheme.

1. Introduction

The Z-source inverter (ZSI) and quasi-Z-source inverter (qZSI) have been employed for PV power generation system due to some unique features and advantages [1–9]. PV panel outputs a fluctuating power due to the variation of solar irradiation and temperature. An energy storage system could be added in the system to smooth the fluctuation of grid-injected power [10–15], where the battery is connected to the system either by an extra DC/DC converter in the DC side or by an extra DC/AC converter in the AC side. These structures make the power generation system more complex and expensive, low efficiency and low reliability.

In [16], application of Z-source inverter to traction drive of fuel cell-battery hybrid electric vehicles was studied, where one of the capacitors in Z-source network was replaced by a battery and the experimental results verified this kind of concept. The same idea can be used to qZSI based PV power system when a battery is connected to a capacitor in parallel. However, with a battery, the qZSI will present different characteristics in terms of operating principle, inductor currents, battery current, capacitor voltages, and dc-link voltage, etc.

This paper will propose a new PV interface inverter through integrating qZSI with battery. Its operating principle, parameter design method, and detailed analysis are investigated. Two control variables, i.e., the shoot-through duty ratio and the modulation index are used to control the output power of PV panel, the power injected to the grid, and the state of charge (SOC) of battery. MPPT algorithm ensures the PV panels' maximum power point (MPP) all the time. Simulation results and experimental results verify the proposed circuit, theoretical analysis, and control scheme.

2. Proposed quasi-Z source inverter with battery and analysis

The qZSI can buck and boost the input voltage in a single stage with two control variables, i.e., the shoot-through duty ratio D and the modulation index M [4–9,17]. If an additional battery is connected to the qZSI network in parallel with a capacitor, the configuration of the qZSI with battery for PV power generation system is shown in Fig. 1.

Equivalent circuits are shown in Figs. 2a and b, when the proposed circuit operates in two state: non-shoot-through state and the shoot-through state, respectively. All the voltages and the currents are defined in Figs. 2a and b. Assuming T is one switching cycle, T_0 is the interval of the shoot-through state; T_1 is the interval of non-shoot-through state; their relationship is $T_0 + T_1 = T$, and the shoot-through duty ratio $D = T_0/T$.

☆ This work was supported in part by the NPRP-Qatar National Research Fund under Grant No. 09-233-2-096, partly by the Beijing Jiaotong University Foundation under Grant No. 2009JBM093, and partly by the State Key Laboratory of Control and Simulation of Power System and Generation Equipments under Grant No. SKLD11KM01, Tsinghua University, Beijing 100084, China.
* Corresponding author.
E-mail addresses: 09117343@bjtu.edu.cn (D. Sun), bm-ge@263.net (B. Ge).

0142-0615/$ - see front matter © 2012 Elsevier Ltd. All rights reserved.
http://dx.doi.org/10.1016/j.ijepes.2012.10.008

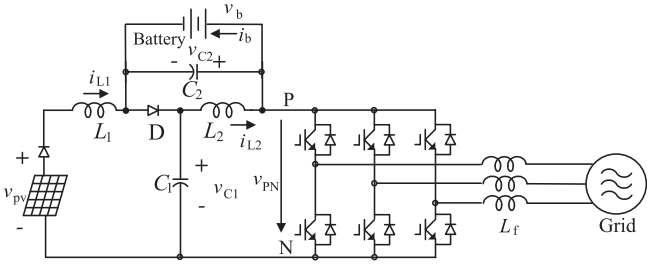

Fig. 1. qZSI with battery for PV system.

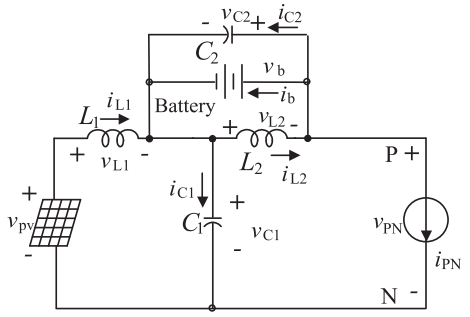

(a) Non-shoot-through state

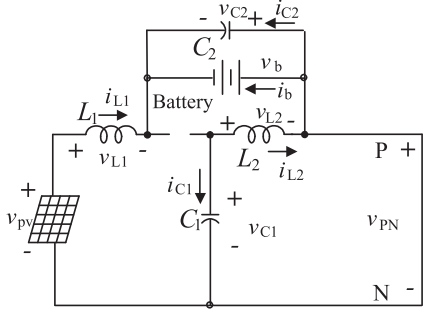

(b) Shoot-through state

Fig. 2. Equivalent circuit of the qZSI with battery.

In Fig. 2a, the inverter operates at the non-shoot-through state T_1. The dynamic equations are

$$\begin{cases} L_1 \frac{di_{L1}}{dt} = v_{pv} - v_{C1} \\ L_2 \frac{di_{L2}}{dt} = -v_{C2} \\ C_1 \frac{dv_{C1}}{dt} = i_{L1} - i_{PN} \\ C_2 \frac{dv_{C2}}{dt} = i_{L2} - i_{PN} - i_b \end{cases} \quad (1)$$

In Fig. 2b, the inverter operates at the shoot-through state T_0. The dynamic equations are

$$\begin{cases} L_1 \frac{di_{L1}}{dt} = v_{pv} + v_{C2} \\ L_2 \frac{di_{L2}}{dt} = v_{C1} \\ C_1 \frac{dv_{C1}}{dt} = -i_{L2} \\ C_2 \frac{dv_{C2}}{dt} = -i_{L1} - i_b \end{cases} \quad (2)$$

In steady state, the average voltages of the inductors over one switching cycle T are zero and the average currents of the capacitors over one switching cycle T are zero. Using (1) and (2), the average voltage and current equations are derived as follows:

$$\begin{cases} L_1 \frac{d\langle i_{L1}\rangle_T}{dt} = (1-D)\cdot(v_{pv} - v_{C1}) + D\cdot(v_{pv} + v_{C2}) = 0 \\ L_2 \frac{d\langle i_{L2}\rangle_T}{dt} = (1-D)\cdot(-v_{C2}) + D\cdot(v_{C1}) = 0 \\ C_1 \frac{d\langle v_{C1}\rangle_T}{dt} = (1-D)\cdot(i_{L1} - i_{PN}) + D\cdot(-i_{L2}) = 0 \\ C_2 \frac{d\langle v_{C2}\rangle_T}{dt} = (1-D)\cdot(i_{L2} - i_{PN} - i_b) + D\cdot(-i_{L1} - i_b) = 0 \end{cases} \quad (3)$$

where the symbol $\langle x\rangle_T$ denotes the average value of instantaneous variable x in the period T.

From (3), the capacitor voltages and inductor currents can be obtained as:

$$\begin{cases} v_{C1} = \frac{1-D}{1-2D} v_{pv} \\ v_{C2} = \frac{D}{1-2D} v_{pv} \end{cases} \quad (4)$$

$$\begin{cases} i_{L1} = \frac{D\cdot i_b + (1-D)\cdot i_{PN}}{1-2D} \\ i_{L2} = \frac{(1-D)\cdot i_b + (1-D)\cdot i_{PN}}{1-2D} \end{cases} \quad (5)$$

The DC-link peak voltage $\hat{v}_{PN}$ can be derived from the sum of two capacitor voltages, v_{C1} and v_{C2}, by:

$$\hat{v}_{PN} = v_{C1} + v_{C2} \quad (6)$$

Two inductor currents i_{L1}, i_{L2}, and the battery current i_b have relationship with

$$i_{L2} - i_{L1} = i_b \quad (7)$$

The PV power can be calculated by:

$$P_{pv} = i_{pv}\cdot v_{pv} = i_{L1}\cdot v_{pv} \quad (8)$$

For battery, its voltage v_b is equal to v_{C2} approximately, if ignoring the voltage drop on the battery internal resistance. So the battery power can be calculated by:

$$P_{battery} = i_b \cdot v_b = i_b \cdot v_{C2} \quad (9)$$

Neglecting the loss of the inverter, the load power is equal to the power flowed into the DC side of the inverter. During the non-shoot-through state T_1, the DC-link voltage across the inverter bridge is

$$v_{PN} = \hat{v}_{PN} \quad (10)$$

During the shoot-through state T_0, the DC-link voltage across the inverter bridge is

$$v_{PN} = 0 \quad (11)$$

Based on (10) and (11), for one switching cycle T, the load power can be expressed by:

$$\begin{aligned} P_{load} &= v_{PN}\cdot i_{PN} = (1-D)\cdot \hat{v}_{PN}\cdot i_{PN} + D\cdot 0 \\ &= (1-D)\cdot \hat{v}_{PN}\cdot i_{PN} \end{aligned} \quad (12)$$

Using (4)–(12), the power relationship in the proposed system can be derived as:

$$P_{pv} - P_{load} = P_{battery} \quad (13)$$

Eqs. (7) and (13) indicate three operating states for the battery: (1) while the battery charging, there are $i_b > 0$, $i_{L2} > i_{L1}$, $P_{battery} > 0$ and $P_{PV} > P_{load}$; (2) while the battery discharging, there are $i_b < 0$, $i_{L2} < i_{L1}$, $P_{battery} < 0$ and $P_{PV} < P_{load}$; and (3) while no charging and discharging, there are $i_b = 0$, $i_{L2} = i_{L1}$, $P_{battery} = 0$ and $P_{PV} = P_{load}$. They are obviously different from traditional qZSI.

3. Parameter design of qZS impedance network

As shown in Fig. 1, the impedance network of the qZSI with battery includes two inductors L_1 and L_2, two capacitors C_1 and C_2, and a diode. Their parameters are designed in the following subsections.

3.1. qZS capacitance design

The qZS capacitors release energy to the qZS inductors during the shoot-through state; while the qZS inductors charge the qZS capacitors during the non-shoot-through state. So during the shoot-through state, we have

$$\Delta v_{C1} = i_{C1}\frac{\Delta t}{C_1} \tag{14}$$

If the carrier frequency is f_s in the system, the switching frequency of the capacitors is doubled with $2f_s$ when using the simple boost control method [4,18]. Therefore, there is

$$\Delta t = \frac{D}{2f_s}, \quad i_{C1} = i_{L2}$$

and the capacitance C_1 can be calculated by:

$$C_1 = i_{L2}\frac{D}{2f_s\Delta v_{C1}} \tag{15}$$

If we set the ripple voltage of qZS capacitors as:

$$\Delta v_{C1,C2} \leqslant a v_{C1,C2} \tag{16}$$

The capacitance C_1 will be

$$C_1 \geqslant i_{L2}\cdot\frac{D}{2f_s a v_{C1}} \tag{17}$$

In the same way, the capacitance C_2 will be

$$C_2 \geqslant i_{L2}\cdot\frac{D}{2f_s a v_{C2}} \tag{18}$$

3.2. qZS inductance design

As the qZS inductors are charged during the shoot-through state, we have

$$\Delta i_{L1} = v_{L1}\frac{\Delta t}{L_1} \tag{19}$$

where

$$\Delta t = \frac{D}{2f_s}, \quad v_{L1} = v_{C1}$$

and the inductance L_1 can be obtained as [4,18]:

$$L_1 = v_{C1}\frac{D}{2f_s\Delta i_{L1}} \tag{20}$$

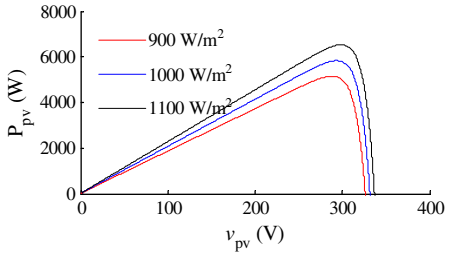

(a) P-V characteristics of the PV panel.

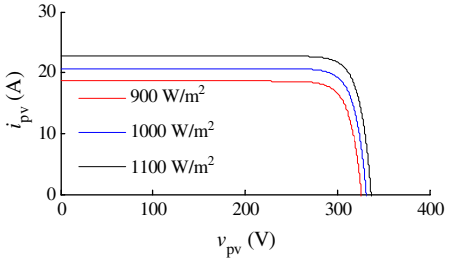

(b) I-V characteristics of the PV panel.

Fig. 4. *P–V* and *I–V* characteristics of the PV panel under different solar irradiation and constant temperature 28 °C.

The qZS inductor's ripple current is defined as:

$$\Delta i_{L1,L2} \leqslant b i_{L1,L2} \tag{21}$$

So the inductance L_1 can be estimated as:

$$L_1 \geqslant v_{C1}\frac{D}{2f_s b i_{L1}} \tag{22}$$

In the same way, the inductance L_2 is calculated by:

$$L_2 \geqslant v_{C1}\frac{D}{2f_s b i_{L2}} \tag{23}$$

3.3. qZS diode design

As shown in Fig. 2, qZS diode is in forward conduction during non-shoot-through state; while it is turned off during shoot-through state because of the negative voltage. So we design the diode according to the voltage stress in shoot-through state and the current stress in non-shoot-through state.

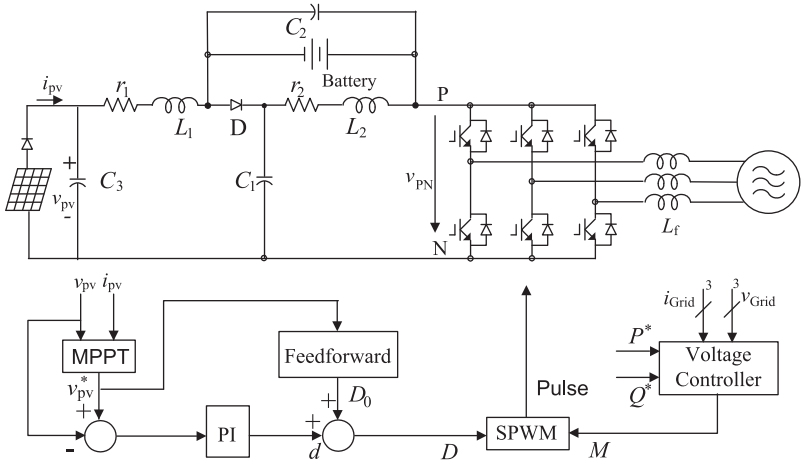

Fig. 3. qZSI-battery PV power system.

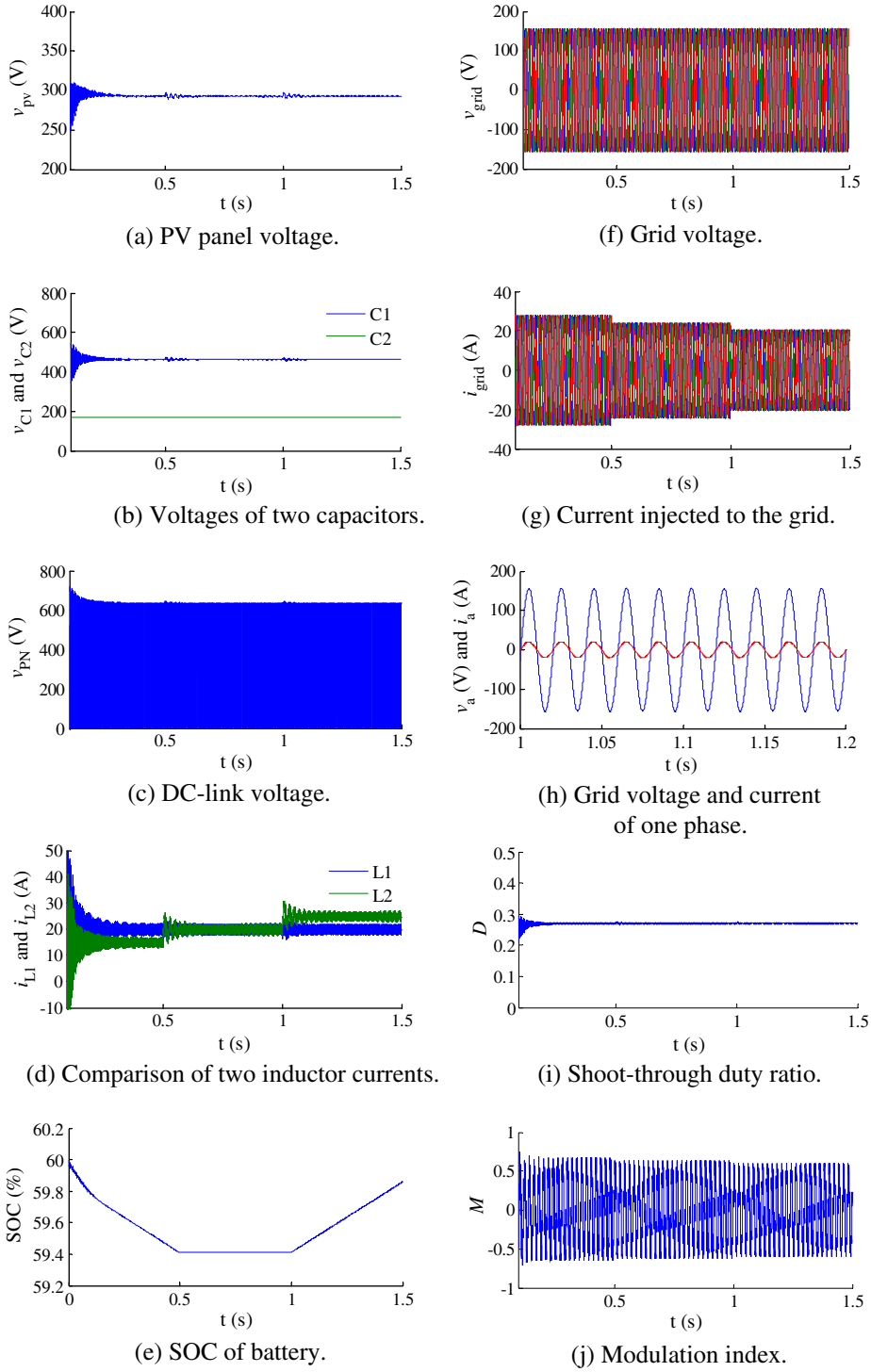

(a) PV panel voltage.
(f) Grid voltage.
(b) Voltages of two capacitors.
(g) Current injected to the grid.
(c) DC-link voltage.
(h) Grid voltage and current of one phase.
(d) Comparison of two inductor currents.
(i) Shoot-through duty ratio.
(e) SOC of battery.
(j) Modulation index.

Fig. 5. Simulation results for the first case.

The voltage stress across the diode in shoot-through state is

$$v_D = v_{C1} + v_{C2} = \hat{v}_{PN} \tag{24}$$

The current flowing through the diode in non-shoot-through state is

$$i_D = i_{L2} + i_{C1} = i_{L1} + i_{L2} - i_{PN} \tag{25}$$

When $i_{PN} = 0$, i_D will obtain the maximum value, so the maximum current of the diode is

$$i_{Dmax} = i_{L1} + i_{L2} \tag{26}$$

4. Proposed PV power system

4.1. Control scheme

The whole proposed PV power system is shown in Fig. 3. In this system, the shoot-through duty ratio D and modulation index M are two control variables. The former is used to achieve the MPPT of PV panel, and the latter is used to control the grid power.

On the DC side, a closed-loop control of PV panel voltage v_{pv} is employed. A proportional and integral regulator with feedforward will adjust D to track the MPP of the PV panel.

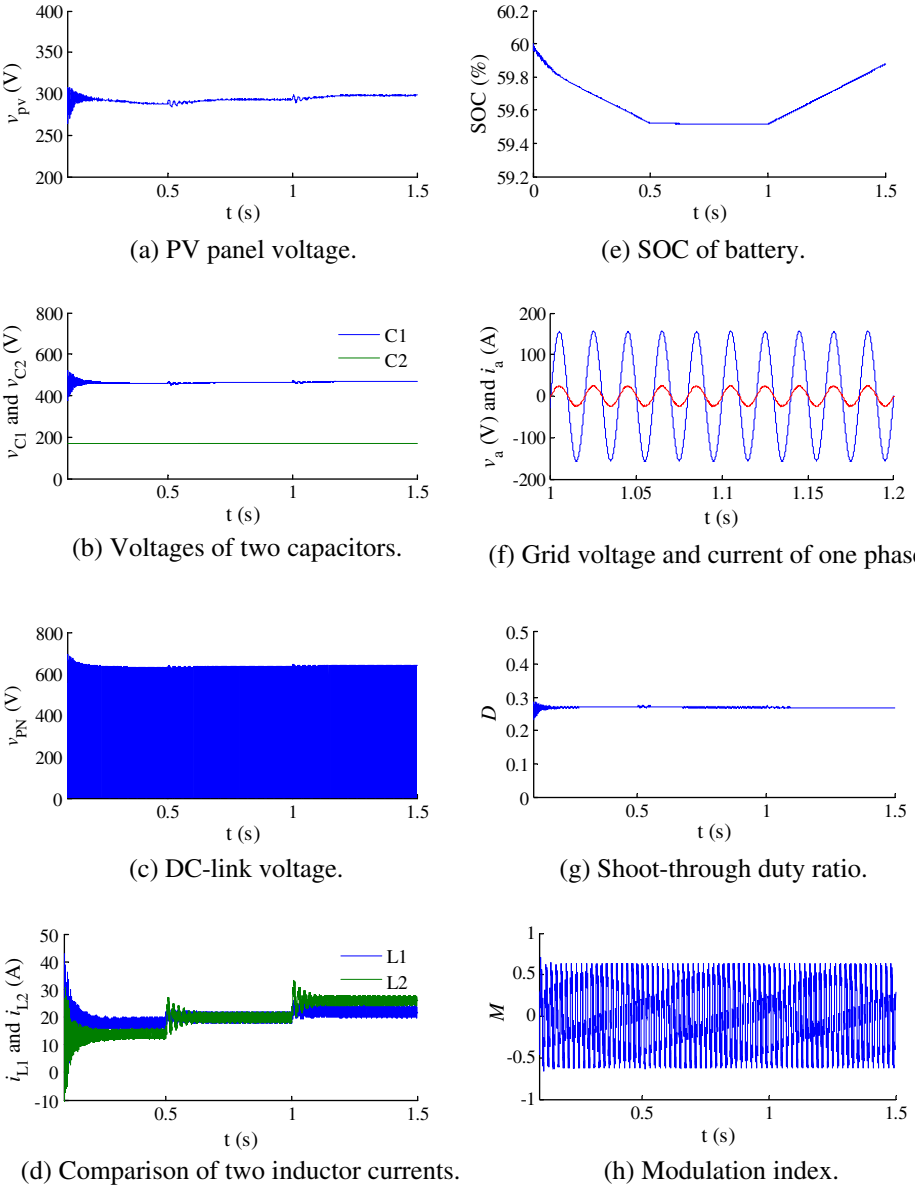

(a) PV panel voltage. (e) SOC of battery.

(b) Voltages of two capacitors. (f) Grid voltage and current of one phase.

(c) DC-link voltage. (g) Shoot-through duty ratio.

(d) Comparison of two inductor currents. (h) Modulation index.

Fig. 6. Simulation results for the second case.

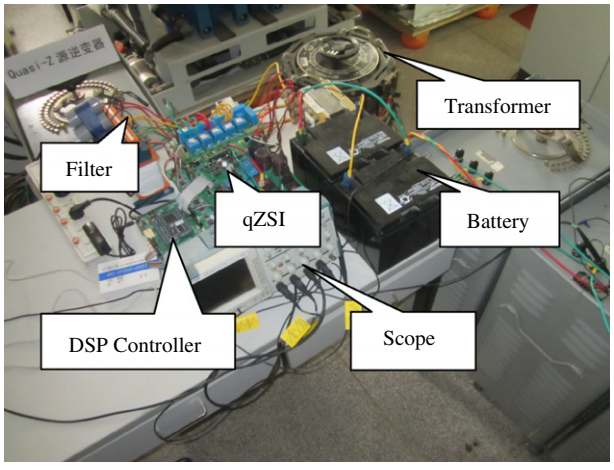

Fig. 7. Experimental setup of the proposed PV system.

On the AC side, the grid-injected active power P and the grid-injected reactive power Q are controlled by the d-axis and q-axis components of the grid currents. Active power P is set on the basis of the actual requirement, while the reactive power Q keeps at zero all the time. The three phase voltages and currents in the grid side are measured and sent to the voltage controller for calculating the modulation index M. M and D are combined together to produce the PWM signals and control the proposed qZSI with battery.

4.2. MPPT algorithm

Fig. 4 shows the P–V and I–V characteristics of the PV panel (KD135GH-2P, 20 × 3 panels) used in simulation. There are different curves when the solar irradiation and temperature are different. The MPPT method being used is the Perturb and Observe (P&O) method [19,20]. In MPPT control, PV voltage and current are measured and inputted to the MPPT block. The PV voltage reference is generated by using P&O algorithm and refreshed every

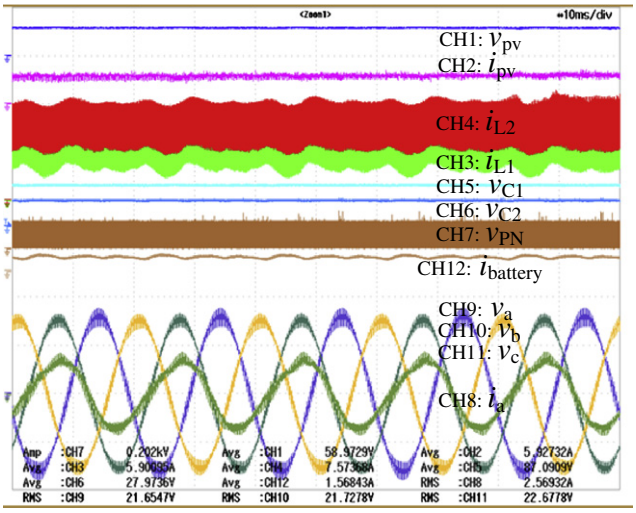

(a) Battery charging mode

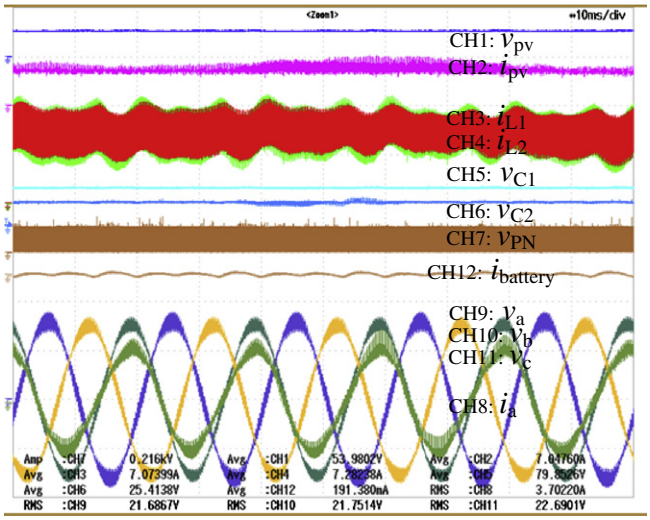

(b) Battery neither charging nor discharging mode

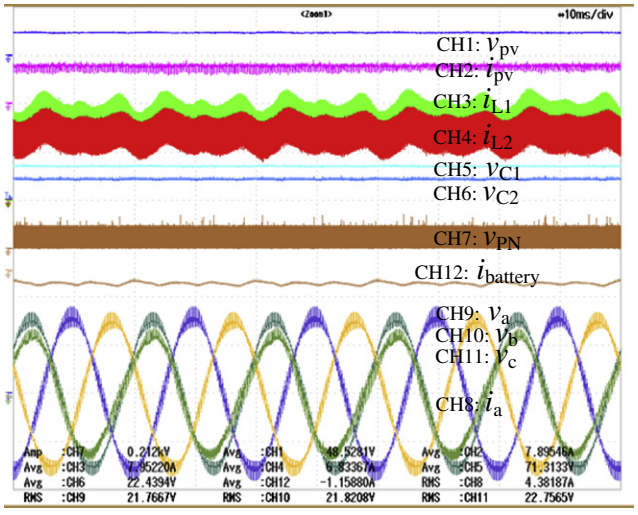

(c) Battery discharging mode

Fig. 8. Experimental results.

0.005 s. For different operating conditions (irradiation and temperature), the PV panel will operate at different MPPs.

5. Simulated results

The proposed energy stored qZSI for PV power generation system is simulated in MATLAB/Simulink. PV panel with type of KD135GH-2P is used in simulations. The designed system parameters are: $L_1 = L_2 = 2$ mH; $C_1 = C_2 = 300$ μF; $C_3 = 1000$ μF; $L_f = 10$ mH; $r_1 = r_2 = 0.01$ Ω. The grid phase voltage is 110 V rms, 50 Hz. A battery with nominal voltage of 170 V is connected in parallel with C_2.

5.1. First case: constant PV power and changeable grid-injected power

In this simulation, the solar irradiation and temperature are kept in 1000 W/m^2, 28 °C, respectively. Given grid-injected active power is 6480 W during 0–0.5 s, 5630 W during 0.5–1 s, and 4780 W during 1–1.5 s. The grid-injected reactive power is always kept in 0 Var.

Fig. 5a shows the PV panel voltage. Even though the power injected to the grid changes, the PV panel always operates at the MPP and provides the constant maximum power to the system. The two capacitor voltages are shown in Fig. 5b. The voltage of capacitor C_2 is nearly constant because of the paralleled battery. The peak DC-link voltage is equal to the sum of v_{C1} and v_{C2}, as shown in Fig. 5c.

Figs. 5d and e show the two inductor currents and battery SOC, respectively. The input current i_{L1} keeps constant, but the current of inductor L_2 varies greatly, which depends on the operating state of the battery. When the PV power is greater than the power injected to the grid during 0–0.5 s, the battery discharges, and there is $i_{L2} < i_{L1}$; when the PV power is equal to the power injected to the grid during 0.5–1 s, the battery keeps no charging and no discharging, and there is $i_{L2} = i_{L1}$; when the PV power is smaller than the power injected to the grid during 1–1.5 s, the battery charges, and there is $i_{L2} > i_{L1}$.

Figs. 5f–h show the grid voltage, the grid current, and the zoomed voltage and current, respectively. The grid voltage is always constant, with 110 V rms, 50 Hz. The grid current varies when the power injected to the grid changes. Although PV power is constant, the grid-injected active power changes from 6480 W during 0–0.5 s, to 5630 W during 0.5–1 s, and to 4780 W during 1–1.5 s, due to the battery's energy storage/release. Fig. 5h shows that the grid voltage and current have the same phase, so the PV grid-connected system presents a unity power factor.

The shoot-through duty ratio D is constant when operated in different modes, as shown in Fig. 5i, which is because of the constant PV panel voltage/power. Fig. 5j shows the modulation signal for SPWM, which presents a little difference for three battery operating states.

5.2. Second case: constant grid-injected power and changeable PV power

Fig. 6 shows the simulation results when the PV power changes due to variation of the solar irradiation, while the grid-injected power keeps in constant. The solar irradiation is $S = 900$ W/m^2 during 0–0.5 s, $S = 1000$ W/m^2 during 0.5–1 s, and $S = 1100$ W/m^2 during 1–1.5 s, but the temperature keeps at $T = 28$ °C. The given grid-injected active and reactive power are 5630 W and 0 Var, respectively.

Fig. 6a shows the PV voltage. It increases when the irradiation changes from 900 W/m^2 to 1100 W/m^2. Figs. 6b and c show the two capacitor voltages and the DC-link voltage.

The two inductor currents in Fig. 6d and the SOC of battery in Fig. 6e show the battery operating states. In simulation, the grid-injected power is kept in 5630 W, and the power difference is balanced by the battery when the PV power is variable. As shown in

Figs. 6d and e, the battery is discharging during 0–0.5 s, no charging and no discharging during 0.5–1 s, and charging during 1–1.5 s.

Fig. 6f shows the grid voltage and current of one phase, and they present unity power factor of PV power system. Fig. 6g shows the shoot-through duty ratio D, which presents a little adjustment in three cases because of the different PV voltage/power. Fig. 6h shows the modulation signal to control the output power.

6. Experimental verification

6.1. Experimental setup

A small-scale power prototype is shown in Fig. 7 to verify the proposed system's functions, including the MPPT algorithm, the grid-injected power control scheme, and the battery charging/discharging. In the tests, the input port of the qZSI with battery is connected to the PV array, which consists of four PV panels (type with KD135GH-2P) in series; and the output is tied to the three-phase grid via a step-up transformer. Two 12 V batteries (lead-acid battery) in series are used as an energy storage device in parallel with the capacitor C_2.

6.2. Experimental results

Fig. 8 shows the experimental results of the proposed system. In the tests, we keep the reactive power at zero, and only change the grid-injected active power to achieve the different operating modes. P&O algorithm is used to implement the MPPT of the PV panels for all tests.

Fig. 8a shows the battery charging mode. The PV array provides more power than the grid-injected power, so the battery is charging. As shown in Fig. 8a, $i_{L2} > i_{L1}$, $i_{battery} = 1.57$ A. Fig. 8b shows the battery with no charging and no discharging mode. For this case, the PV array provides the exact power injected to the grid, so the battery is neither charging nor discharging, with $i_{L2} = i_{L1}$, $i_{battery} = 0$ A; Fig. 8c shows the battery discharging state, where the PV power is less than the grid-injected power, and $i_{L2} < i_{L1}$, $i_{battery} = -1.16$ A.

7. Conclusion

A quasi-Z-source inverter with battery for photovoltaic power generation system was proposed. In this system the battery was paralleled with one of the capacitors directly to store or release energy, without any extra components. The power conversion circuit of qZSI with battery system was analyzed. The relationships among PV power, battery power, and inverter power, and among two inductor currents and battery current were derived. A simple control method achieved the PV panel's MPPT, and the management of battery SOC through controlling the power injected to the grid. The simulation results and experimental results verified the proposed energy stored qZSI, theoretical analysis, and the control scheme.

References

[1] Huang Y, Shen MS, Peng FZ, Wang J. Z-source inverter for residential photovoltaic systems. IEEE Trans Power Electron 2006;21(6):1776–82.
[2] Badin R, Huang Y, Peng FZ, Kim HG. Grid interconnected Z-source PV system. In: Proceedings of IEEE power electronics specialists conference, Orlando, USA; 2007. p. 2328–33.
[3] Jinjun Huang, Jianyong Zheng, Jun You, et al. Z-source three-phase grid-connected PV system based on current hysteresis control. Electr Power Autom Equip 2010;30(10):94–7.
[4] Li Y, Anderson J, Peng FZ, Liu DC. Quasi-Z-source inverter for photovoltaic power generation systems. In: Proceedings of the twenty-fourth annual IEEE applied power electronics conference and exposition, Washington (DC, USA); 2009. p. 918–24.
[5] Bradaschia F, Cavalcanti MC, Ferraz PEP, Neves FAS, dos Santos EC, da Silva JHGM. Modulation for three-phase transformerless Z-source inverter to reduce leakage currents in photovoltaic systems. IEEE Trans Indust Electron 2011;58(12):5385–95.
[6] Vinnikov D, Roasto I. Quasi-Z-source-based isolated DC/DC converters for distributed power generation. IEEE Trans Indust Electron 2011;58(1):192–201.
[7] Anderson J, Peng FZ. Four quasi-Z-source inverters. In: Proceedings of IEEE power electronics specialists conference, Rhodes, Greece; 2008. p. 2743–9.
[8] Park JH, Kim HG, Nho EC, Chun TW, Choi J. Grid-connected PV system using a quasi-Z-source Inverter. In: Proceedings of the twenty-fourth annual IEEE applied power electronics conference and exposition, Washington (DC, USA); 2009. p. 925–9.
[9] Li Y, Peng FZ, Cintron-Rivera JG, Jiang S. Controller design for quasi-Z-source inverter in photovoltaic systems. In: Proceeding of energy conversion congress and exposition, Atlanta, USA; 2010. p. 3187–94.
[10] Bo D, Li YD, Zheng ZD. Energy management of hybrid DC and AC bus linked microgrid. In: Proceedings of power electronics for distributed generation systems, Hefei, China; 2009. p. 713–6.
[11] Tina GM, Pappalardo F. Grid-connected photovoltaic system with battery storage system into market perspective. In: Proceedings of sustainable alternative energy, Valencia, Spain; 2009. p. 1–7.
[12] Wang WL, Ge BM, Bi DQ, Sun DS. Grid-connected wind farm power control using VRB-based energy storage system. In: Proceeding of energy conversion congress and exposition, Atlanta, USA; 2010. p. 3772–7.
[13] Jayasinghe SDG, Vilathgamuwa DM, Madawala UK. A battery energy storage interface for wind power systems with the use of grid side inverter. In: Proceeding of energy conversion congress and exposition, Atlanta, USA; 2010. p. 3786–91.
[14] Ge Baoming, Wang Wenliang, Bi Daqiang, Rogers Craig B, et al. Energy storage system-based power control for grid-connected wind power farm. Int J Electr Power Energy Syst 2013;44(1):115–22.
[15] Sebastian R. Modelling and simulation of a high penetration wind diesel system with battery energy storage. Int J Electr Power Energy Syst 2011;33(3):747–67.
[16] Peng FZ, Shen MS, Holland K. Application of Z-source Inverter for traction drive of fuel cell – battery hybrid electric vehicles. IEEE Trans Power Electron 2007;22(3):1054–61.
[17] Peng FZ. Z-source inverter. IEEE Trans Indust Appl 2003;39(2):504–10.
[18] Hsieh Hung-I, Chang Chin-Hao, Hsieh Guan-Chyun. A study of fuel cell Z-source boost converter: considerations on design and implementation. In: Proceedings of power electronics and drive systems, Singapore; 2011. p. 441–6.
[19] Hengsritawat Vichakorn, Tayjasanant Thavatchai, Nimpitiwan Natthaphob. Optimal sizing of photovoltaic distributed generators in a distribution system with consideration of solar radiation and harmonic distortion. Int J Electr Power Energy Syst 2012;39(1):36–47.
[20] Kabalci Ersan, Kabalci Yasin, Develi Ibrahim. Modelling and analysis of a power line communication system with QPSK modem for renewable smart grids. Int J Electr Power Energy Syst 2012;34(1):36–47.